Unsteady Effects on Pathological Droplet-fueled Detonations

Raúl Hernández-Sánchez[1], Jaime Carpio-Huertas[2], Daniel Martínez-Ruiz[2], César Huete[1]
[1]Universidad Carlos III de Madrid, Leganés, Madrid, Spain
[2]Universidad Politécnica de Madrid, Madrid, Spain

1 Introduction

The understanding of detonation fundamentals is a topic of great interest for the design and development of high-speed propulsion systems, such as Scramjets and Rotating Detonation Engines (RDEs) [4]. However, most classical studies on gaseous detonations are insufficient to capture the intrinsic dynamics arising from the interaction between liquid-fuel sprays and the detonation structure [5].

The global thermodynamic balance is commonly envisioned to provide the self-propagating conditions of the Chapman-Jouguet (CJ) regime, the Mach number M_{CJ} and downstream properties of the flow such as temperature, pressure and kinetic energy, for a given mixture of prescribed initial conditions. However, when incorporating liquid-phase fuel into the detonation process, additional mechanisms involving heating and evaporation of the liquid phase must be accounted for to remove a non-negligible amount of energy from the budget to sustain the detonation. The total available energy in the upstream state is characterized by the thermodynamic variables and the mass-loading ratio of the disperse phase to carrier gas, α. The classical zero-dimensional global conservation balance already fails in the purpose of predicting the propagation speed of liquid-fueled detonations when confronted to models that account for the inner structure of the two-phase interaction.

Furthermore, recent 2D/3D numerical simulations [6] highlight the intricate nature of detonation dynamics, incorporating droplet vaporization through a droplet-shock interaction model. However, they neglect the influence of droplet interaction with the flow during vaporization, heating, and accommodation. These primary physical processes governing such a complex reactive flow were addressed in [1] within a steady one-dimensional theoretical framework, using an Eulerian-Eulerian approach to model the key challenges associated with monodisperse liquid-fuel spray usage. This formulation has also identified pathological regimes in which a significant portion of the heat release and fuel vaporization occurs beyond the CJ sonic point. Consequently, these late processes fail to influence the detonation, thereby altering its self-sustained velocity [2].

In the present study, the multiphase formulation accounting for mass, momentum and energy exchange is extended to incorporate unsteady effects using a 2D finite-element solver that treats the dispersed liquid phase as Lagrangian particles undergoing vaporization. Specially, we shall focus on the unsteady effects arising in the pathological detonation regimes mentioned above. To complete the picture, the simulations presented in this work are crucial for understanding transient and oscillatory regimes in two-phase detonations, as well as for characterizing the canonical dynamics locally influenced by droplet inertia and clustering effects.

Correspondence to: raulhern@ing.uc3m.es

2 Problem Formulation

The unsteady one-dimensional detonation structure is studied in a moving reference frame attached to the shock, propagating with the CJ velocity of the steady self-sustained regime. This value $D_{\mathrm{CJ}}^{\mathrm{eigen}}$ is computed as described in [2], accounting for the heat required for vaporization of the liquid fuel. Therefore, an inflow of gaseous oxidizer with velocity $D_{\mathrm{CJ}}^{\mathrm{eigen}}$ transports a liquid phase consisting of a monodisperse spray of fuel droplets of radius a. The mass-loading ratio of the disperse phase to the carrier gas in absence of prevaporized fuel can be written as $\alpha = \phi/s \sim \mathcal{O}(1)$, and is determined by the overall equivalence ratio ϕ and the amount of oxidizer mass consumption per unit fuel mass burnt s. Consequently, given the large droplet-to-gas density ratio $\rho_d/\rho \sim \mathcal{O}\left(10^3\right)$, a low liquid volume fraction $\psi \sim \mathcal{O}\left(\rho_{\mathrm{d}}/(\rho\alpha)\right) \ll 1$ is ensured. This justifies a dilute spray approximation, where droplet interactions and collisions are neglected.

The two-way coupled gas-droplet system is here described using an Eulerian-Lagrangian framework, with the gas phase computed on an Eulerian grid and the droplets modeled as N_{d} discrete Lagrangian point particles. The gas phase is described by a thermally perfect ideal gas model with $p = \rho RT$ and $e = c_v T$. The Euler conservation equations for mass, momentum, total energy $E = e + |\boldsymbol{v}|^2/2$, fuel vapor species Y_{F}, and oxidizer species Y_{O}, respectively, read

$$\frac{\partial \rho}{\partial t} + \boldsymbol{\nabla}\cdot(\rho\boldsymbol{v}) = -\sum_{k=1}^{N_{\mathrm{d}}} \delta_k \frac{\mathrm{d}m_k}{\mathrm{d}t}, \tag{1}$$

$$\frac{\partial}{\partial t}(\rho\boldsymbol{v}) + \boldsymbol{\nabla}\cdot(\rho\boldsymbol{v}\boldsymbol{v}) + \boldsymbol{\nabla}p = -\sum_{k=1}^{N_{\mathrm{d}}} \delta_k \frac{\mathrm{d}}{\mathrm{d}t}(m_k\boldsymbol{v}_k), \tag{2}$$

$$\frac{\partial}{\partial t}(\rho E) + \boldsymbol{\nabla}\cdot[(\rho E + p)\,\boldsymbol{v}] = -\sum_{k=1}^{N_{\mathrm{d}}} \delta_k \frac{\mathrm{d}}{\mathrm{d}t}\left(m_k c T_k - m_k L_{\mathrm{v}} + \frac{1}{2} m_k |\boldsymbol{v}_k|^2\right) + Q\dot{\omega}, \tag{3}$$

$$\frac{\partial}{\partial t}(\rho Y_{\mathrm{F}}) + \boldsymbol{\nabla}\cdot(\rho Y_{\mathrm{F}}\boldsymbol{v}) = -\sum_{k=1}^{N_{\mathrm{d}}} \delta_k \frac{\mathrm{d}m_k}{\mathrm{d}t} - \dot{\omega}, \tag{4}$$

$$\frac{\partial}{\partial t}(\rho Y_{\mathrm{O}}) + \boldsymbol{\nabla}\cdot(\rho Y_{\mathrm{O}}\boldsymbol{v}) = -s\dot{\omega}, \tag{5}$$

where the source terms on the right-hand side describe the mass, momentum, and energy exchange with the k^{th} droplet in the liquid phase and the reaction rate $\dot{\omega}$. These two-way exchanges between phases take place at the position $\boldsymbol{x}_k$ of each droplet through the Dirac delta distribution $\delta_k = \delta(\boldsymbol{x} - \boldsymbol{x}_k)$. Finally, the chemical kinetics follows an irreversible one-step Arrhenius law, $\dot{\omega} = B\rho Y_{\mathrm{F}} Y_{\mathrm{O}} \exp(-E_{\mathrm{a}}/RT)$, where B is the pre-exponential factor, and E_{a} the activation energy.

This reactive gas problem must be solved together with the disperse phase, where the temporal evolution of the position, radius, velocity, and temperature of each droplet is governed by the following ODEs [3],

$$\frac{\mathrm{d}\boldsymbol{x}_k}{\mathrm{d}t} = \boldsymbol{v}_k, \tag{6}$$

$$\frac{\mathrm{d}m_k}{\mathrm{d}t} = \frac{4}{3}\pi\rho_{\mathrm{d}}\frac{\mathrm{d}a_k^3}{\mathrm{d}t} = \dot{m}_k, \tag{7}$$

$$m_k\frac{\mathrm{d}\boldsymbol{v}_k}{\mathrm{d}t} = \frac{4}{3}\pi a_k^3\rho_{\mathrm{d}}\frac{\mathrm{d}\boldsymbol{v}_k}{\mathrm{d}t} = \boldsymbol{f}_k, \tag{8}$$

$$m_k c\frac{\mathrm{d}T_k}{\mathrm{d}t} = \frac{4}{3}\pi a_k^3\rho_{\mathrm{d}} c\frac{\mathrm{d}T_k}{\mathrm{d}t} = \dot{q}_k, \tag{9}$$

with c representing the specific heat of the liquid phase. These evolution equations incorporate the vaporization rate $\dot{m}_k$, the drag force exerted by the gas $\boldsymbol{f}_k$, and the heating rate $\dot{q}_k$ experienced by the droplet. These terms for each individual droplet can be respectively computed by

$$\dot{m}_k = -4\pi a_k \frac{k}{c_p}\lambda_k, \qquad \boldsymbol{f}_k = 6\pi\mu a_k(\boldsymbol{v}-\boldsymbol{v}_k), \qquad \dot{q}_k = 4\pi k a_k \left(\frac{T-T_k}{e^{\lambda_k}-1} - \frac{L_\mathrm{v}}{c_p}\right)\lambda_k, \tag{10}$$

with $\lambda_k = \log[(1-Y_\mathrm{F})/(1-Y_{\mathrm{F},k})]/\mathrm{Le}_\mathrm{F}$ the dimensionless vaporization rate, determined by the balance of convective and diffusive heat and mass transfer between the gas and the surface of the droplet. The mass fraction of fuel vapor on the droplet surface $Y_{\mathrm{F},k}$ is computed through the Clausius-Clapeyron relation

$$Y_{\mathrm{F},k} = \frac{W_\mathrm{F}}{W_\mathrm{s}} \exp\left(\frac{L_\mathrm{v}}{RT_\mathrm{B}} - \frac{L_\mathrm{v}}{RT_k}\right), \tag{11}$$

with T_B the boiling temperature at the post-shock pressure, W_F the molecular mass of the vapor fuel and $W_\mathrm{s} = (\Sigma_i Y_{i,\mathrm{s}}/W_i)^{-1}$ the molecular mass of the mixture at the droplet surface. The boiling temperature and latent heat of vaporization L_v are taken constant for the sake of simplicity, given that the limited variations of pressure in the post-shock region yield modifications in the boiling temperature through the saturation line of less than 10%. Additionally, the Stokes drag force is considered if the slip velocity $(\boldsymbol{v}-\boldsymbol{v}_k)$ renders a small droplet-based Reynolds number $(\mathrm{Re}_\mathrm{d} \ll 1)$. Although this may not always be the case in the droplet detonation scenario, incorporation of large Reynolds dynamics through a drag coefficient and dependence on the velocity difference squared does not modify the qualitative behavior addressed here. Similarly, even if the d^2-law based vaporization model may limit the quantitative accuray of the results, the qualitative description of the two-way coupling dynamics is not modfied by the use of more detailed vaporization models. Finally, $\lambda_k/(e^{\lambda_k}-1)$ is the Nusselt number of the associated Steffan flow for an evaporating sphere.

The chemical reaction characterizes the induction time, $t_\mathrm{i} = \beta_0^{-1}\mathrm{e}^{\beta_0}/B$, through the Zel'dovich number $\beta_0 = E_\mathrm{a}/RT_{0,\mathrm{CJ}}$, where $T_{0,\mathrm{CJ}}$ is the postshock temperature in CJ conditions. It should be noted that this value is dependent on the propagating state of the configuration M_CJ, that is reached for a given setup of the two-phase mixture, equivalence and mass loading ratios. However, β_1 will be analogously referred to upstream preshock conditions, which remains unchanged with variations of the detonation propagation solution, but does not appropriately describe the scaling of the induction time.

Figure 1 presents the steady-state pathological detonation diagram in the $\phi - \beta_1$ space as a function of the Stokes number,

$$\mathrm{St} = \frac{t_\mathrm{a}}{t_\mathrm{i}} = \frac{2}{9}\frac{\rho_\mathrm{d}}{\rho}\frac{\beta_0}{\mathrm{e}^{\beta_0}}\frac{Ba_0^2}{\nu}, \tag{12}$$

which relates the inertia-related droplet accommodation time, for an initial droplet radius a_0 at the postshock stage, to the induction time, following the analysis in [1]. Under sufficiently rich conditions, an increase in the Stokes number favors the onset of pathological behavior [2]. Direct inspection of Fig. 1 also reveals that the pathological condition domain expands for higher activation energy values. Since sufficiently large β_1 values may lead to instability, assessing the detonation's dynamic behavior is essential, as addressed numerically in the following section.

3 Numerical Integration

The system of coupled conservation equations for the gaseous phase eqs. (1) to (5) and the disperse phase eqs. (6) to (9) are numerically integrated with an in-house finite element solver. The numerical method is based on a Lagrange-Galerkin conservative weak formulation of the equations [7]. For temporal discretization, a second-order Explicit Runge-Kutta-Chebyshev method is employed [8], whose main

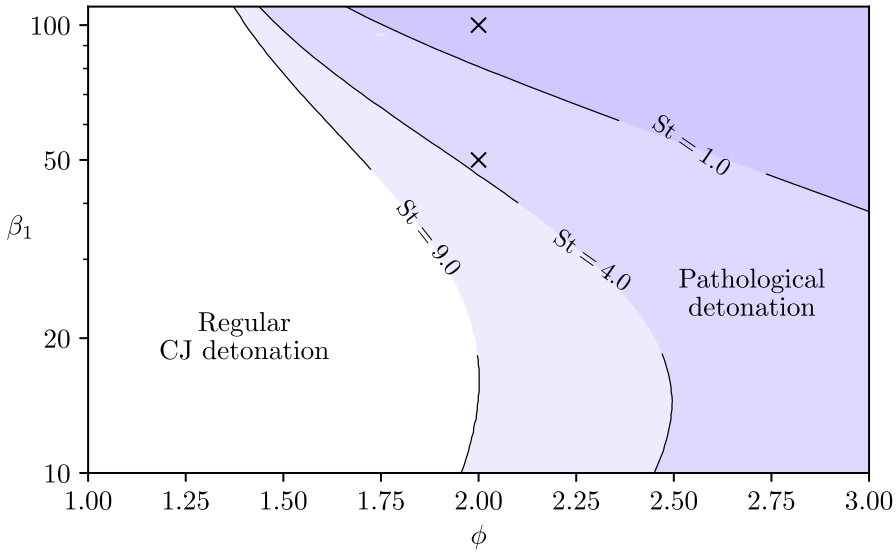

Figure 1: Pathological detonation diagram in the $\phi - \beta_1$ space as a function of the Stokes number obtained with the Eulerian-Eulerian formulation in [2]. Markers indicate the conditions studied in Fig.3.

advantage is that it enhances stability by increasing the number of stages in the algorithm. For spatial discretization, an anisotropic, locally adaptive finite element methodology with quadratic polynomials is used. The two-dimensional domain is deliberately slender to preserve a predominantly one-dimensional behavior. The streamwise length is $L_x = 75$ and the transverse height is $L_y = 0.5$, defined in terms of the gas-induction length $l_\mathrm{i} = u_0 t_\mathrm{i}$, where u_0 represents the velocity of the post-shock fluid relative to the shock wave. A minimum element size of $h = 0.02$ is applied around the shock region. The temporal integration domain is $[0, 325]$, with a time step of $\Delta t = 0.01$, with the characteristic time taken as t_i. This results in a CFL number of 0.5.

The number of discrete droplets is $N_\mathrm{d} = 500$ per unit time, injected in equilibrium conditions with the carrier gas at the inlet boundary. Thus, 5 droplets are injected each time step with a uniform probability distribution over the $y-$direction domain $[0, 0.5]$. Under the studied cases, this results in approximately 35.000 droplets within the computational domain. This ensures a transverse-averaged behavior that reproduces the one-dimensional Eulerian-Eulerian results of the earlier steady state works [1, 2]. The numerical simulation is initialized with the pathological steady-state solution obtained in [2]. Boundary conditions involve the upstream supersonic flow at the inlet $x = 0$, zero gradient on the burnt outlet $x = L_x$ and slip walls on $y = 0$ and $y = L_y$.

4 Results

First, we shall show a multicontinua steady-state solution compared to the transient numerical simulation detailed above. Figure 2 shows the ZND spatial distribution of dimensionless pressure, temperature, fuel and oxidant mass fractions, and Mach number as function of the dimensionless spatial coordinate for moderately large inertial droplets with $\mathrm{St} = 4$, and fuel-rich mixture $\phi = 2$. A careful choice of the parameters investigated has been made to illustrate the pathological regimes considering a generic fuel. The Zel'dovich number is $\beta_1 = 50$. This case corresponds to a pathological detonation, as shown in Fig. 1 that includes the two branches of feasible steady solutions. The chemical reaction can accelerate the flow after the shock, which reaches a sonic point. However, the transonic region must coincide with the zero thermicity locus of the post-shock evolution [2]. After the sonic point either a subsonic or

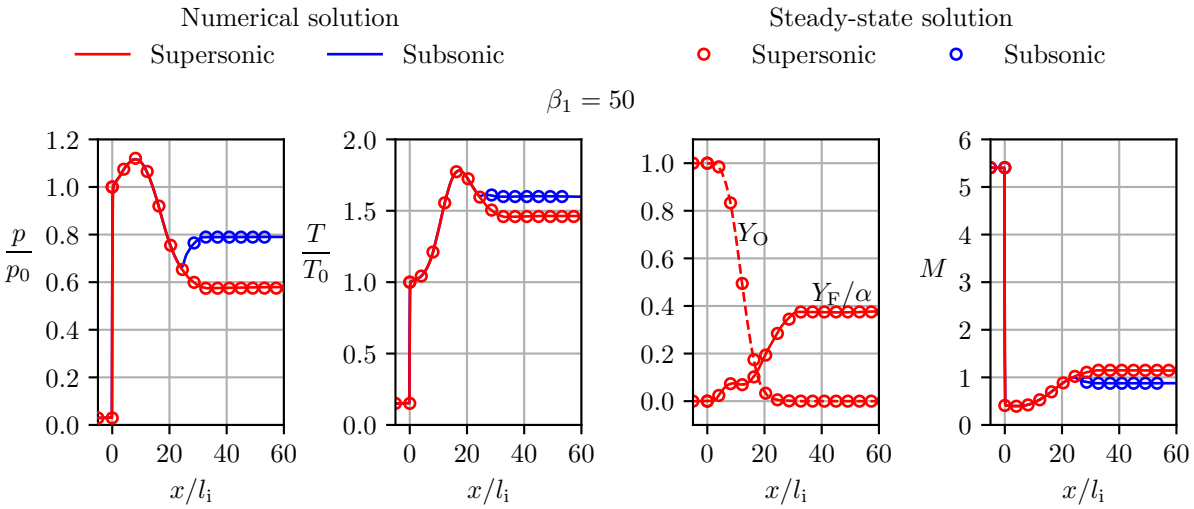

Figure 2: Dimensionless pressure p/p_0, temperature T/T_0, reduced fuel vapor Y_F/α and oxidant Y_O mass fractions, and Mach number M over the streamwise coordinate x/l_i in the ZND structure of a droplet-fueled pathological detonation. Steady-state solutions (empty bullets) are compared with the $y-$averaged numerical simulations (solid line).

a supersonic branch could take place, depicted in both separate branches, for the same CJ state given that the events in after the sonic point do not affect nor contribute to the propagation of the detonation front. The transient y-averaged numerical integration (solid lines) is initialized with both supersonic and subsonic downstream flow conditions provided by the steady-state equations (empty bullets), and in both cases, a steady state condition is maintained over time.

A similar analysis for $\beta_1 = 100$, initiated from the steady-state solution under both supersonic and subsonic far-field branches, reveals a dynamic detonation wave response characterized by the well-known one-dimensional oscillations associated with high activation energies. To further investigate this unsteady behavior, Fig. 3 shows the time evolution of the shock front position and the out-of-equilibrium region. This region is characterized by three key points: the location where the limiting reactant is consumed x_r, where sonic conditions are reached x_s, and where the droplets are completely vaporized x_d. Results are presented for $\beta_1 = 50$ (left panel) and $\beta_1 = 100$ (right panel), showing the evolution of both the supersonic (red) and subsonic (blue) solution branches. It is observed that as the activation energy is increased, small variations in the temperature of the field can produce great changes in the reaction rate, giving rise to the characteristic galloping detonation state. However, stable oscillating solutions have not been obtained in the parametric space tested here, where the initial response typically grows and progressively decouples the shock and reaction layer, which translates into the effective decay of the detonation structure.

5 Conclusions

This study builds on previous work [2], which showed that steady pathological detonations are feasible when fuel encounters the shock in small droplets. Under sufficiently rich conditions, endothermic fuel vaporization near the end of the non-equilibrium region may occur after the sonic plane has formed within the thermally neutral zone. The presence of this sonic locus decouples the detonation from downstream conditions, allowing it to propagate independently. Moreover, the sonic locus isolates part of the endothermic contribution, causing the propagation speed to exceed the prediction of the integral formula a widely used methodology that fails to account for the non-contributing endothermic region.

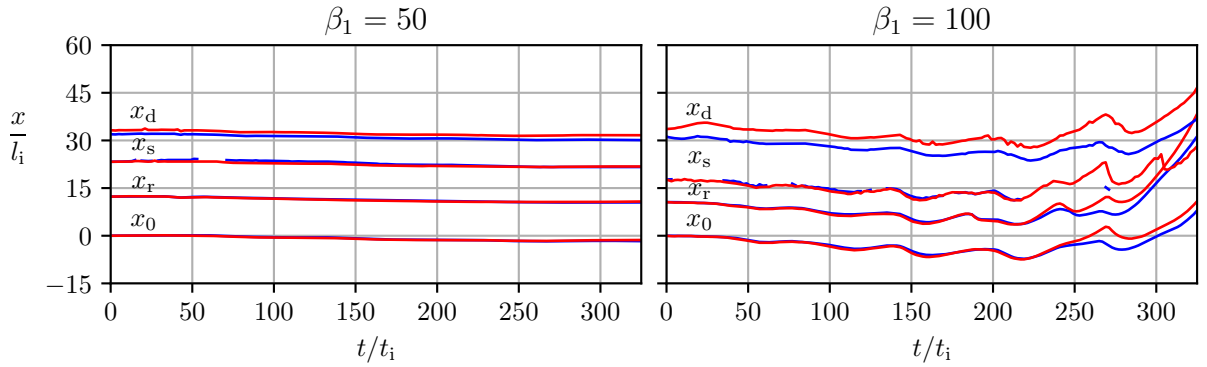

Figure 3: Temporal evolution of the shock wave x_0, end of reaction zone x_r, sonic point x_s and end of vaporization zone x_d position in a droplet-fueled pathological detonation for $\beta_1 = 50$ (left) and $\beta_1 = 100$ (right), showing supersonic (red) and subsonic (blue) solution branches.

This work extends previous findings by numerically solving the dynamic response under one-dimensional conditions using an in-house numerical code to solve conservation equations in an Eulerian-Lagrangian framework. Variations in the dimensionless activation energy, characterized by the factor β_1, can lead to unsteady configurations that initially oscillate and lead to decoupled shock and reaction layers. For the pathological cases analyzed, we observe that unstable behavior emerges at higher β_1 values in liquid-fueled detonations compared to analogous gas-phase detonations, highlighting the stabilizing effect of the vaporization process.

References

[1] Martínez-Ruiz D (2023). On the structure of the steady one-dimensional liquid-fueled detonations. Phys. Fluids 35: 086122.

[2] Hernández-Sánchez R., Huete C., & Martínez-Ruiz D. (2024). Pathological detonations in monodisperse spray media. Proc. Combust. Inst. 40: 105505.

[3] Sánchez AL, Urzay J, Liñán A. (2015). The role of separation of scales in the description of spray combustion. Proc. Combust. Inst. 35: 1549-1577.

[4] Raman, V., Prakash, S., & Gamba, M. (2023). Nonidealities in rotating detonation engines. Annu. Rev. Fluid Mech., 55(1), 639-674.

[5] Yao, S., Guo, C., & Zhang, W. (2023). Effects of droplet evaporation on the flow field of hydrogen-enhanced rotating detonation engines with liquid kerosene. Int. J. Hydrogen Energy, 48(85), 33335-33345.

[6] Dammati, S. & Poludnenko, A. & Kateris, N. & Dong, W. & Wang, H. & Lu, T. (2025). Numerical Simulations of Non-Ideal Spray Detonations in Jet Fuels With a Shock-Droplet Interaction Model. AIAA SCITECH 2025 Forum.

[7] Colera, M. & Carpio, J. & Bermejo R. (2020). A nearly-conservative high-order Lagrange–Galerkin method for the resolution of scalar convection-dominated equations in non-divergence-free velocity fields. Comput. Methods Appl. Mech. Eng. 372, 113366.

[8] Carpio, J. & Prieto, J.L. & Galán del Sastre, P. (2019). An anisotropic adaptive, Lagrange-Galerkin numerical method for spray combustion. J. Comp. Phys. 381, 246 - 274.